https://doi.org/10.5607/en.2018.27.6.550
Exp Neurobiol. 2018 Dec;27(6):550-563.
pISSN 1226-2560 • eISSN 2093-8144

Original Article

Experimental Neurobiology

Check for updates

A *De Novo RAPGEF2* Variant Identified in a Sporadic Amyotrophic Lateral Sclerosis Patient Impairs Microtubule Stability and Axonal Mitochondria Distribution

Keunjung Heo[1†], Su Min Lim[2†], Minyeop Nahm[2†], Young-Eun Kim[3], Ki-Wook Oh[2], Hwan Tae Park[4], Chang-Seok Ki[5*], Seung Hyun Kim[2*] and Seungbok Lee[1*]

[1]Department of Brain and Cognitive Sciences and Dental Research Institute, Seoul National University, Seoul 08826, [2]Department of Neurology, College of Medicine, Hanyang University, Seoul 04763, [3]Department of Laboratory Medicine, College of Medicine, Hanyang University, Seoul 04763, [4]Department of Molecular Neuroscience, College of Medicine, Dong-A University, Busan 49201, [5]Green Cross Genome Corporation, Yongin 16924, Korea

Amyotrophic lateral sclerosis (ALS) is a fatal neurodegenerative disease that is frequently linked to microtubule abnormalities and mitochondrial trafficking defects. Whole exome sequencing (WES) of patient-parent trios has proven to be an efficient strategy for identifying rare *de novo* genetic variants responsible for sporadic ALS (sALS). Using a trio-WES approach, we identified a *de novo RAPGEF2* variant (c.4069G>A, p.E1357K) in a patient with early-onset sALS. To assess the pathogenic effects of this variant, we have used patient-derived skin fibroblasts and motor neuron-specific overexpression of the RAPGEF2-E1357K mutant protein in *Drosophila*. Patient fibroblasts display reduced microtubule stability and defective microtubule network morphology. The intracellular distribution, ultrastructure, and function of mitochondria are also impaired in patient cells. Overexpression of the RAPGEF2 mutant in *Drosophila* motor neurons reduces the stability of axonal microtubules and disrupts the distribution of mitochondria to distal axons and neuromuscular junction (NMJ) synapses. We also show that the recruitment of the pro-apoptotic protein BCL2-associated X (BAX) to mitochondria is significantly increased in patient fibroblasts compared with control cells. Finally, increasing microtubule stability through pharmacological inhibition of histone deacetylase 6 (HDAC6) rescues defects in the intracellular distribution of mitochondria and BAX. Overall, our data suggest that the *RAPGEF2* variant identified in this study can drive ALS-related pathogenic effects through microtubule dysregulation.

Key words: Amyotrophic lateral sclerosis, Whole exome sequencing, *RAPGEF2*, Missense mutation, Microtubules, Mitochondria

Received October 31, 2018, Revised November 24, 2018, Accepted November 26, 2018

*To whom correspondence should be addressed.
Chang-Seok Ki, TEL: 82-31-260-0601, FAX: 82-31-260-9087, e-mail: changski.md@gmail.com
Seung Hyun Kim, TEL: 82-2-2290-8371, FAX: 82-2-2296-8370, e-mail: kimsh1@hanyang.ac.kr
Seungbok Lee, TEL: 82-2-880-2330, FAX: 82-2-762-2583, e-mail: seunglee@snu.ac.kr
†These authors contributed equally to this work.

INTRODUCTION

Amyotrophic lateral sclerosis (ALS) is a progressive neurodegenerative disease that affects both upper and lower motor neurons, leading to muscle weakness and atrophy followed by paralysis [1, 2]. ALS is usually fatal due to respiratory failure within 5 years after symptom onset and represents the most common form of adult-onset motor neuron diseases with an incidence of 2 per 100,000. Approximately 10% of cases show familial inheritance, while the remaining majority of cases occur sporadically. Over the last two decades, substantial progress has been made in understanding of the genetic landscape of familial ALS (fALS). To date, two-thirds of fALS are associated with mutations in any of more than 25 genes [3-5], encoding proteins involved in protein homeostasis, RNA metabolism, vesicular trafficking, and cytoskeletal organization. Despite this progress in identifying fALS-associated genes, the genetic etiology of sporadic ALS (sALS) remains largely unknown [3].

Impaired mitochondrial trafficking in motor neurons is a well-established phenomenon in ALS pathophysiology [6]. Electron microscopic studies of post-mortem ALS cases demonstrated remarkable accumulation of mitochondria in the somata and proximal axons of motor axons in the spinal cord [7]. Consistently, abnormal clustering of mitochondria in proximal axons of motor neurons was also observed in transgenic mice and rats expressing the ALS mutant SOD1-G93A [8, 9]. Similar defects in mitochondrial distribution were also observed in motor neurons from transgenic mice expressing ALS-associated TDP-43 mutants [10, 11]. However, the underlying mechanisms of mitochondrial trafficking defects in ALS remain to be fully understood.

Whole exome sequencing (WES) has significantly contributed to our knowledge of ALS genetics. First, WES studies on ALS families identified novel pathogenic variants in known fALS genes, including *SOD1*, *SPG11*, and *UBQLN2* [12-14]. Second, the WES analysis of ALS families or in large ALS cohorts discovered new fALS genes such as *VCP*, *PFN1*, *hnRNPA1*, *NEK1*, and *TBK1* [15-19]. Finally, a previous WES-based study on family trios (the affected person and his/her parents) identified a *de novo* variant in the new sALS gene *SS18L1* (also known as *CREST*) that was subsequently found to be associated with two fALS cases [20, 21], demonstrating the power of WES to identify new ALS-associated genes.

In this study, we employed a trio-WES approach to identify pathogenic variants in a sALS patient and detected a *de novo* missense variant (c.4069G>A, p.E1357K) in the *RAPGEF2* gene. Our data obtained from patient-derived fibroblasts and a *Drosophila* model expressing the mutant protein suggests that the RAPGEF2 variant identified in this study impairs mitochondrial distribution and morphology through microtubule dysregulation, which has been increasingly recognized as a core component of ALS pathogenesis [22].

MATERIALS AND METHODS

Subjects, exome sequencing, and genetic variant analysis

The 28-year-old female patient and her healthy parents provided written informed consent as approved by the Institutional Review Boards of Hanyang University Hospital (Seoul, Korea). Genomic DNA was isolated from peripheral blood leukocytes using the Wizard Genomic DNA Purification kit (Promega, Madison, WI, USA). The exomes of subjects were captured using the Agilent SureSelect all Exon 50Mb kit (Agilent, Santa Clara, CA, USA) and sequenced on an Illumina NextSeq500 machine (paired-end and 100-bp reads) (Illumina, San Diego, CA, USA). Reads were mapped to a custom GRCh37/hg19 build using the Burrows-Wheeler Aligner (BWA). Annotation was performed using an in-house custom-made script. We selected rare variants with allele frequency less than 0.01 identified in the NHLBI Exome Sequencing Project (http://evs.gs.washington.edu/EVS/), the 1000 Genomes Project (http://www.1000genomes.org/), and gnomAD (http://gnomad.broadinstitute.org/). All amino acid-altering *de novo* variants with filtering criteria were validated by Sanger sequencing on DNA samples from the family trio using primers designed by the authors.

Molecular biology and cell culture

Full-length cDNAs for *RAPGEF2* and *Bcl-2-associated X protein* (*BAX*) were PCR-amplified from total human cDNAs and cloned into the pEGFP-C1 vector (Clontech, Mountain View, CA, USA) to generate *pEGFP-RAPGEF2* and *pEGFP-BAX*. The E1357K mutation was introduced into *pEGFP-RAPGEF2* by PCR-mediated mutagenesis to produce *pEGFP-RAPGEF2-E1357K*.

Primary human fibroblasts were established from punch biopsies on the forearm skin of the patient and a 43-year-old male control as described previously [23] and maintained in Dulbecco's modified Eagle's medium (DMEM) containing 20% heat-inactivated (30 min, 55°C) fetal bovine serum (FBS), 1% non-essential amino acids, and antibiotics. Passage-matched control and patient fibroblasts (prior to passage 10) were used in each experiment. For inhibition of HDAC6, human skin fibroblasts were treated with 1 μM tubastatin A (Sigma-Aldrich, St. Louis, MI, USA) overnight at 37°C. Human HeLa cells were maintained in DMEM supplemented with 10% heat-inactivated FBS and transfected using FuGENE HD transfection reagent (Promega, Madison, WI, USA).

Fly strains

Flies were maintained at 25°C on standard food. Transgenic *D42-GAL4* and *D42-GAL4,UAS-mito-HA-GFP* flies were obtained from the Bloomington Stock Center (Bloomington, IN, USA). The *UAS-HA-RAPGEF2-WT* and *UAS-HA-RAPGEF2-E1357K* transgenes were produced in the w^{1118} background by standard germline transformation. The RNAi line PDZ-GEF^{KK102612} (referred to here as to *UAS-gef26*^{RNAi}) was obtained from the Vienna *Drosophila* Resources Center (Vienna, Austria).

Immunostaining, imaging, and quantification

Cultured cells were fixed with 4% formaldehyde in PBS for 20 min at room temperature, permeabilized with 0.2% Triton X-100 in PBS for 10 min, and blocked with 1% BSA in PBS for 1 h. Samples were then incubated with primary antibodies for 1 h and sequentially incubated with fluorescently labeled secondary antibodies for 30 min at room temperature. Wandering third-instar *Drosophila* larvae were dissected in Ca^{2+}-free HL3 saline, fixed with 4% formaldehyde in PBS for 20 min, and immunostained as previously described [24]. The following primary antibodies were used in this study: anti-mitochondria (1:1000; Millipore, Burlington, MA, USA), anti-acetylated α-tubulin (1:500; Sigma-Aldrich), anti-tyrosinated α-tubulin (1:500; Millipore, Bedford, MA, USA), anti-α-tubulin (1:500; Sigma-Aldrich), and anti-Futsch (1:50; DSHB, Iowa City, IA, USA). The FITC-, Cy3-, and Cy5-conjugated secondary antibodies were obtained from Jackson ImmunoResearch (1:200; West Grove, PA, USA).

Fluorescent images were acquired with an LSM 700 laser-scanning confocal microscope using a C Apo 40x W or Plan Apo 63x 1.4 NA objective (Carl Zeiss, Jena, Germany). The length of Mito-RFP-labeled mitochondria in fibroblasts was determined using ImageJ. For quantification of the number and area of mitochondria in *Drosophila* motor neurons, we acquired confocal images of A5 segment in dissected third instar larvae labeled with anti-GFP (for Mito-GFP) and anti-HRP antibodies. The number and area of Mito-GFP puncta normalized to the respective area were also determined using ImageJ as previously described [25].

Adult behavioral analysis

A climbing test was used to assess the locomotor function of adult flies as previously described [24]. Briefly, 45 adult flies aged for 20 days were transferred into a glass graduated cylinder. Following 5-min acclimation, flies were gently tapped to the bottom and the distance climbed by individual flies in a 30 s period was measured.

Western blot analysis

Primary human skin fibroblasts were homogenized in ice-cold lysis buffer (50 mM Tris-HCl, pH 7.4, 150 mM NaCl, 1% Triton X-100, and protease inhibitors) and subjected to western blotting as previously described [23]. For some experiments, we separated the mitochondrial and cytosolic fractions from fibroblast lysates using the BioVision Mitochondria/Cytosol Fractionation kit (BioVision, Milpitas, CA, USA). The following primary antibodies were used: anti-acetylated α-tubulin (1:1000; Sigma-Aldrich), anti-tyrosinated α-tubulin (1:1000; Millipore), anti-α-tubulin (1:1000; Sigma-Aldrich), anti-BAX (1:1000; BD, Franklin Lakes, NJ, USA), and anti-GAPDH (1:1000; Santa Cruz Biotechnology, Dallas, TX, USA).

Analysis of mitochondrial membrane potential

The mitochondrial membrane potential was assessed in live primary fibroblasts using 5,5',6,6'-tetrachloro-1,1',3,3'-tetraethylbenzimidazolylcarbocyanine iodide (JC-1; Sigma-Aldrich) as described [26]. Briefly, fibroblasts were washed and incubated with 5 μg/ml JC-1 dye for 20 min at 37°C. The cells were then rinsed with culture medium, and their images were obtained using the Applied Precision DeltaVision fluorescence microscopy system (GE Healthcare, Chicago, IL, USA). JC-1 accumulates as red fluorescent aggregates within polarized mitochondria but does as green fluorescent monomers within less polarized mitochondria.

Electron microscopy

Primary human skin fibroblasts were fixed in PBS containing 4% paraformaldehyde and 2.5% glutaraldehyde for 24 h and rinsed in PBS. The samples were then subjected to 70-nm sectioning after gradual dehydration in ethanol solutions and propylene oxide (Acros Organics, Morris Plains, NJ, USA), and stained with epoxy resins using standard procedures. Images were acquired with a Hitachi electron microscope (Hitachi, Tokyo, Japan) equipped with a ES500W digital camera (GATAN, Pleasanton, CA, USA).

Statistical analysis

Comparisons were made by one-way ANOVA analysis with a post-hoc Turkey test. Data are presented as mean±SEM.

RESULTS

Identification of a de novo variant in the RAPGEF2 gene in a sALS patient

While performing WES on sALS trios, we identified a 28-year-old female patient carrying a *de novo* variant in the *RAPGEF2* gene (c.4069G>A, p.E1357K) (Fig. 1A). The *de novo* occurrence

https://doi.org/10.5607/en.2018.27.6.550

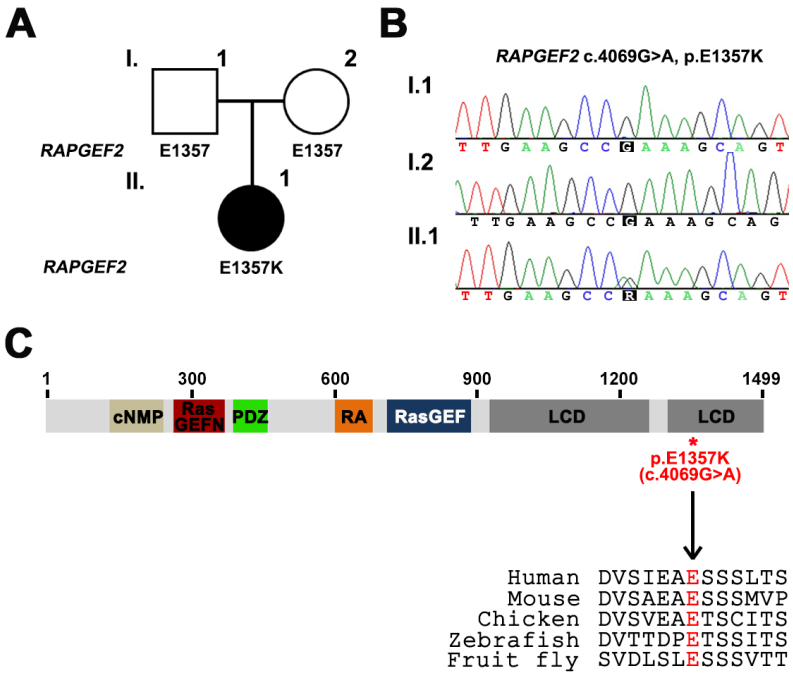

Fig. 1. Detection of a *RAPGEF2 de novo* variant (p.E1357K) in a sALS trio. (A) Family pedigree. Square indicates male; circle, female; and solid, affected. (B) Confirmation of the p.E1357K variant in *RAPGEF2* by Sanger sequencing. (C) Domain architecture of the human RAPGEF2 protein along with the position of the identified substitution. Conserved domains are identified by SMART (Simple Modular Architecture Research Tool, http://smart.embl-heidelberg.de) and PONDR (Predictor of Natural Disordered Regions, http://www.pondr.com). The asterisk indicates the position of the substitution p.E1357K within the second LCD domain of RAPGEF2. Note that the amino acid E1357 is highly conserved among species. cNMP, cyclic nucleotide monophosphate-binding; Ras-GEFN, the N-terminal domain of guanine nucleotide exchange factor for Ras-like GTPases; PDZ, PSD-95/Dlg/ZO-1 binding domain; RA, Ras/Rap association; RasGEF, guanine nucleotide exchange factor for Ras-like GTPases; LCD, low-complexity domain.

of this variant in the patient was confirmed by Sanger sequencing (Fig. 1B). In addition, we proved no additional pathogenic variants in the most common fALS genes including *C9orf72*, *SOD1*, *FUS*, *TARDBP*, and *TBK1*. She developed progressive weakness first in the lower limbs and then in the upper limbs from 27 years of age. The neurologic examination at our clinic showed clinical signs of upper motor neuron involvement, mild hand wasting, and fasciculation in the lower limbs. Needle electromyography (EMG) showed widespread active denervation potentials with fasciculation in both upper and lower limbs. In addition, we observed long-duration, large-amplitude polyphasic potentials during volitional contraction, suggesting that there is chronic re-innervation. Based on the revised El Escorial criteria [27], she was diagnosed with clinically probable ALS.

The *RAPGEF2* gene encodes a Rap1-specific guanine nucleotide exchange factor (GEF) that harbors an N-terminal cyclic nucleotide monophosphate-binding (cNMP) domain, a Ras-GEFN domain, a PSD-95/Dlg/ZO-1 (PDZ) domain, a Ras association (RA) domain, and a RasGEF domain, which is followed by two C-terminal low-complexity domains (LCDs). Previous studies have shown that ALS-causing mutations are frequently found in the LCD domains of RNA-binding proteins, including TDP-43, FUS, hnRNP A1, and TIA1 [28-30]. The RAPGEF2-E1357 residue is highly conserved among species ranging from *Drosophila* to vertebrates and locates within the second LCD domain (Fig. 1C).

Reduction of the stable microtubule network in patient-derived skin fibroblasts carrying the E1357K variant of RAPGEF2

Disruptions in microtubule network assembly have been proposed as a critical component of ALS pathogenesis [22]. We therefore asked whether the E1357K variant of RAPGEF2 affects microtubule dynamics or organization. To address this, we visualized microtubule networks in control- and patient-derived skin fibroblasts using antibodies against α-tubulin (detecting both free α-tubulin and microtubules), acetylated α-tubulin (detecting long-lived, stable microtubules [31]), and tyrosinated α-tubulin (detecting both free tubulin and newly formed microtubules [32]). In control cells, all of these tubulin antibodies revealed the typical microtubule pattern of an aster-like distribution extending toward the cell periphery (Fig. 2A). The levels and distribution of α-tubulin and tyrosinated α-tubulin remained unchanged in patient fibroblasts (Fig. 2A). In sharp contrast, anti-acetylated α-tubulin signals were weaker in patient fibroblasts than in control fibroblasts (Fig. 2A). In addition, acetylated α-tubulin networks were restricted only in the perinuclear region. We confirmed the selective reduction of acetylated α-tubulin in patient cells by western blotting (Fig. 2B~D). These results suggest that the E1357K variant of RAPGEF2 affects the stability of the microtubule network.

To corroborate the above conclusion, we analyzed the effect of the RAPGEF2-E1357K variant on the level of α-tubulin acetylation in HeLa cells. Levels of anti-acetylated α-tubulin signal were

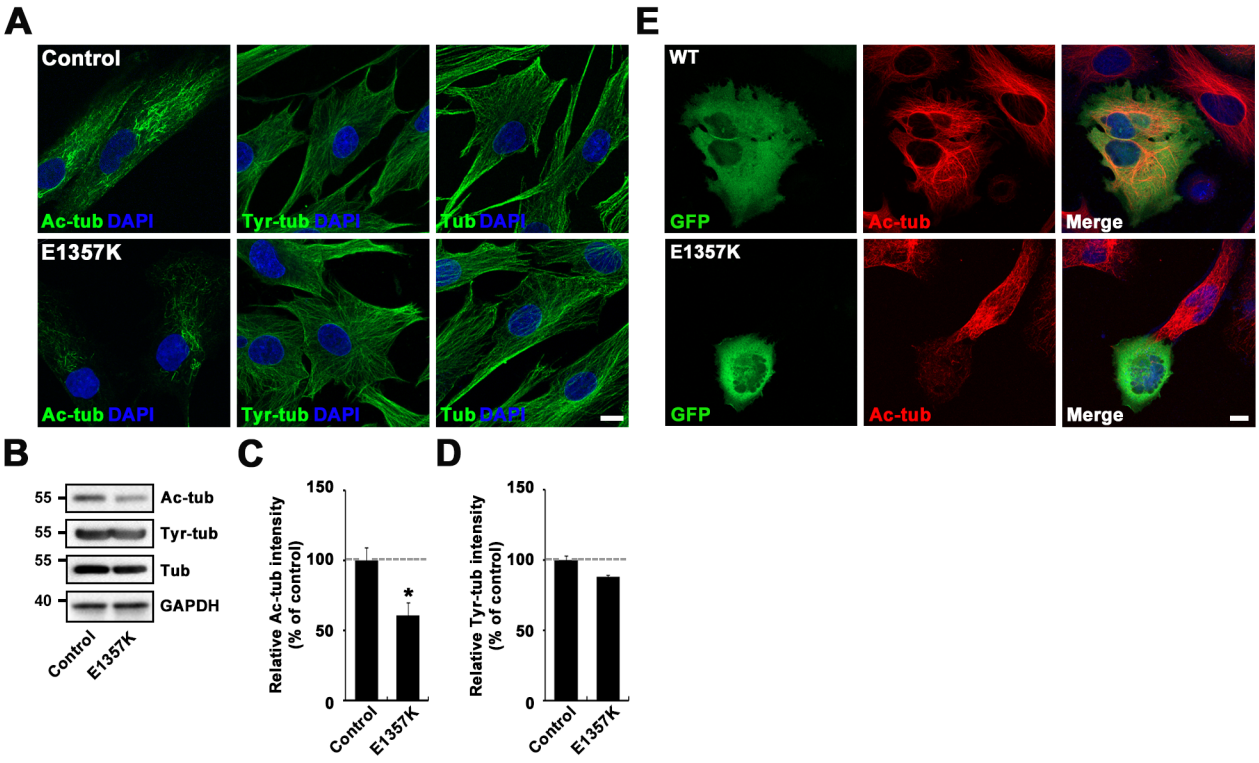

Fig. 2. ALS patient-derived fibroblasts display reduced levels of acetylated α-tubulin and disrupted microtubule network. (A) Confocal images of control-derived fibroblasts and ALS patient-derived fibroblasts (E1357K) labeled with antibodies against acetylated α-tubulin (Ac-tub), tyrosinated α-tubulin (Tyr-tub), or α-tubulin (Tub) and DAPI. Scale bar, 5 μm. (B) Western blot analysis of lysates from control and patient fibroblasts using anti-acetylated α-tubulin, anti-tyrosinated α-tubulin, anti-α-tubulin, and anti-GAPDH antibodies. (C and D) Quantitative analysis by densitometric measurements (n=3). The intensities of Ac-tub and Tyr-tub were normalized to that of Tub. Data are presented as mean±SEM. *p<0.001. (E) Confocal images of HeLa cells transiently expressing wild-type GFP-RAPGEF2 (WT) or GFP-RAPGEF2-E1357K (E1357K) labeled with anti-GFP and anti-Ac-tub antibodies. Note that the microtubule network is disrupted in GFP-RAPGEF2-E1357K-expressing cells but not in GFP-RAPGEF2-expressing cells. Scale bar, 5 μm.

significantly decreased in RAPGEF2-E1357K-transfected cells compared with untransfected control cells (Fig. 2E), confirming a deleterious effect of the RAPGEF2 variant on microtubule stability.

Abnormal mitochondrial distribution in patient fibroblasts

Since appropriate mitochondrial distribution critically depends on microtubule-based transport, we investigated whether alteration of the microtubule network in patient-derived fibroblasts is paralleled with abnormalities in mitochondrial morphology and distribution. Control and patient fibroblasts were transfected with a mitochondrial matrix-localized RFP (Mito-RFP) reporter construct. In control cells, Mito-RFP signals largely appeared as tubular networks extending throughout the cytoplasm (Fig. 3A). In contrast, the Mito-RFP-labeled mitochondria networks in patient-derived cells were fragmented and more restricted around the perinuclear area (Fig. 3A). To quantify mitochondrial fragmentation, we measured mitochondrial length. Patient fibroblasts showed a reduction of about 88% in average mitochondrial length compared with control cells (Fig. 3B). However, the size of cells was comparable between both genotypes (Fig. 3C).

Next, we investigated whether the decrease in the stability of microtubules is a causative mechanism of abnormal mitochondrial distribution in patient-derived fibroblasts. Acetylation of lysine 40 in α-tubulin, an indication of microtubule stabilization, is increased by inhibiting the catalytic activity of histone deacetylase 6 (HDAC6) [33], which is the major deacetylase of α-tubulin [34]. We examined the effect of an HDAC6-selective inhibitor (tubastatin A) on mitochondrial distribution in patient fibroblasts. Treatment of fibroblasts with 1 μM tubastatin A restored abnormalities in acetylated α-tubulin distribution and mitochondrial distribution and length (Fig. 3A~C). These results suggest that impaired microtubule stability is a causative mechanism accounting for abnormal mitochondrial distribution in patient-derived fibroblasts expressing the RAPGEF2-E1357K variant.

https://doi.org/10.5607/en.2018.27.6.550

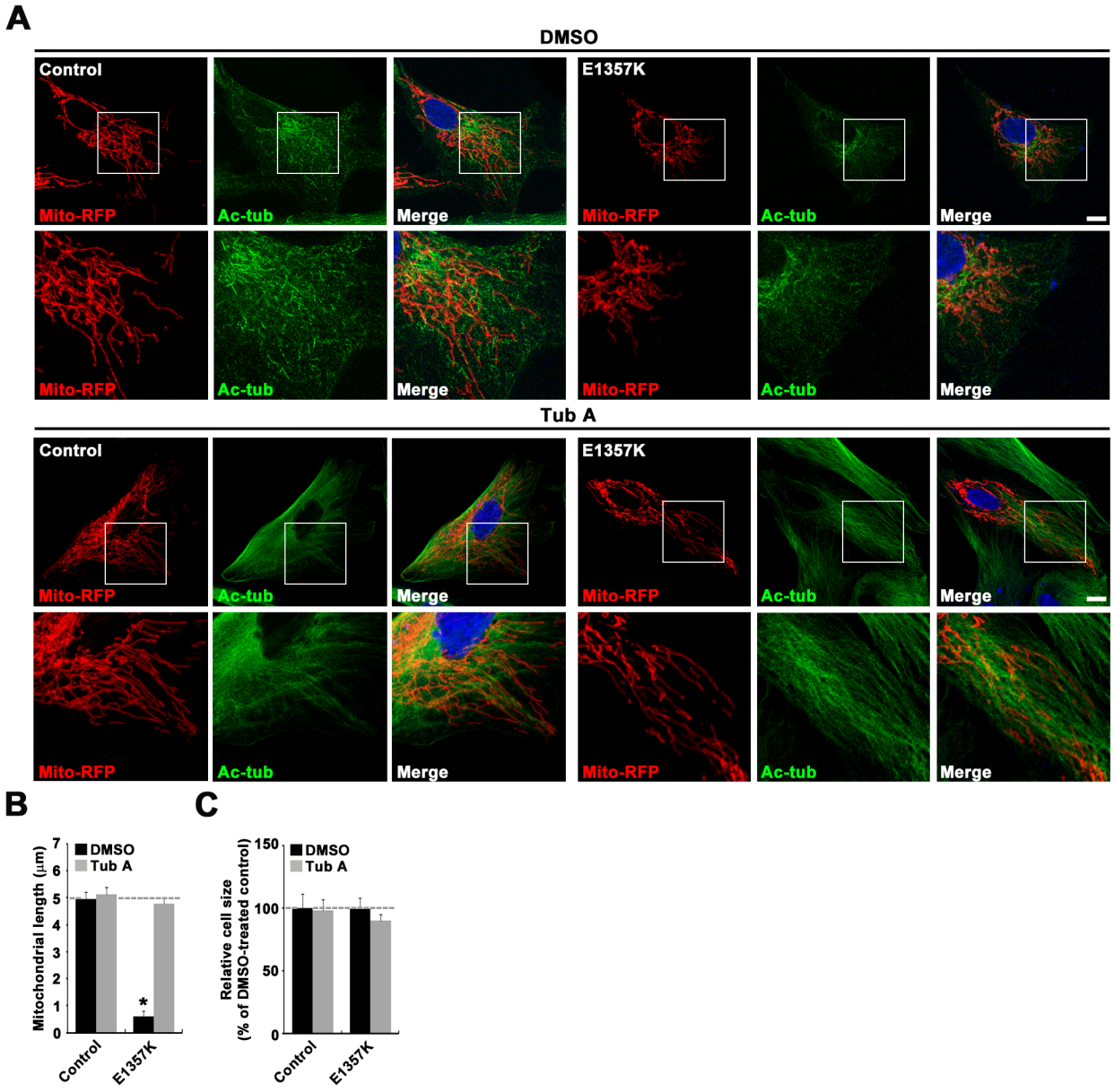

Fig. 3. Pharmacological inhibition of HDAC6 rescues abnormalities in the mitochondrial network in ALS patient-derived fibroblasts carrying the RAPGEF2-E1357K variant. (A) Confocal images of Mito-RFP-expressing control and patient (E1357K) fibroblasts treated with DMSO or 1 μM tubastatin A (Tub A). Cells were labeled with anti-acetylated α-tubulin (Ac-tub) and DAPI. Bottom panels show higher magnification views of the regions marked by boxes. Scale bar, 5 μm. (B and C) Quantification of mitochondria length and cell size (n=7 for DMSO-treated control fibroblasts; n=6 for DMSO-treated patient fibroblasts (E1357K); n=11 for Tub A-treated control fibroblasts; n=11 for Tub A-treated patient fibroblasts (E1357K). Data are presented as mean±SEM. Comparisons are made with DMSO-treated control fibroblasts (*p<0.001).

Transgenic expression of the RAPGEF2-E1357K variant in Drosophila motor neurons impairs microtubule stability and mitochondria distribution along axons

To validate the effects of the RAPGEF2-E1357K mutant on microtubule maintenance and mitochondrial distribution in motor axons, we generated *Drosophila* carrying UAS transgenes of HA-tagged wild-type RAPGEF2 (*UAS-HA-RAPGEF2-WT*) and its E1357K mutant (*UAS-HA-RAPGEF2-E1357K*). We targeted expression of these transgenes in larval motor neurons using the *D42-GAL4* driver. First, we performed confocal analysis on third instar larvae with antibodies against acetylated α-tubulin and Futsch, a microtubule-associated protein stabilizing microtubules [35]. Both acetylated α-tubulin and Futsch staining in motor axons and neuromuscular junction (NMJ) synapses were not altered

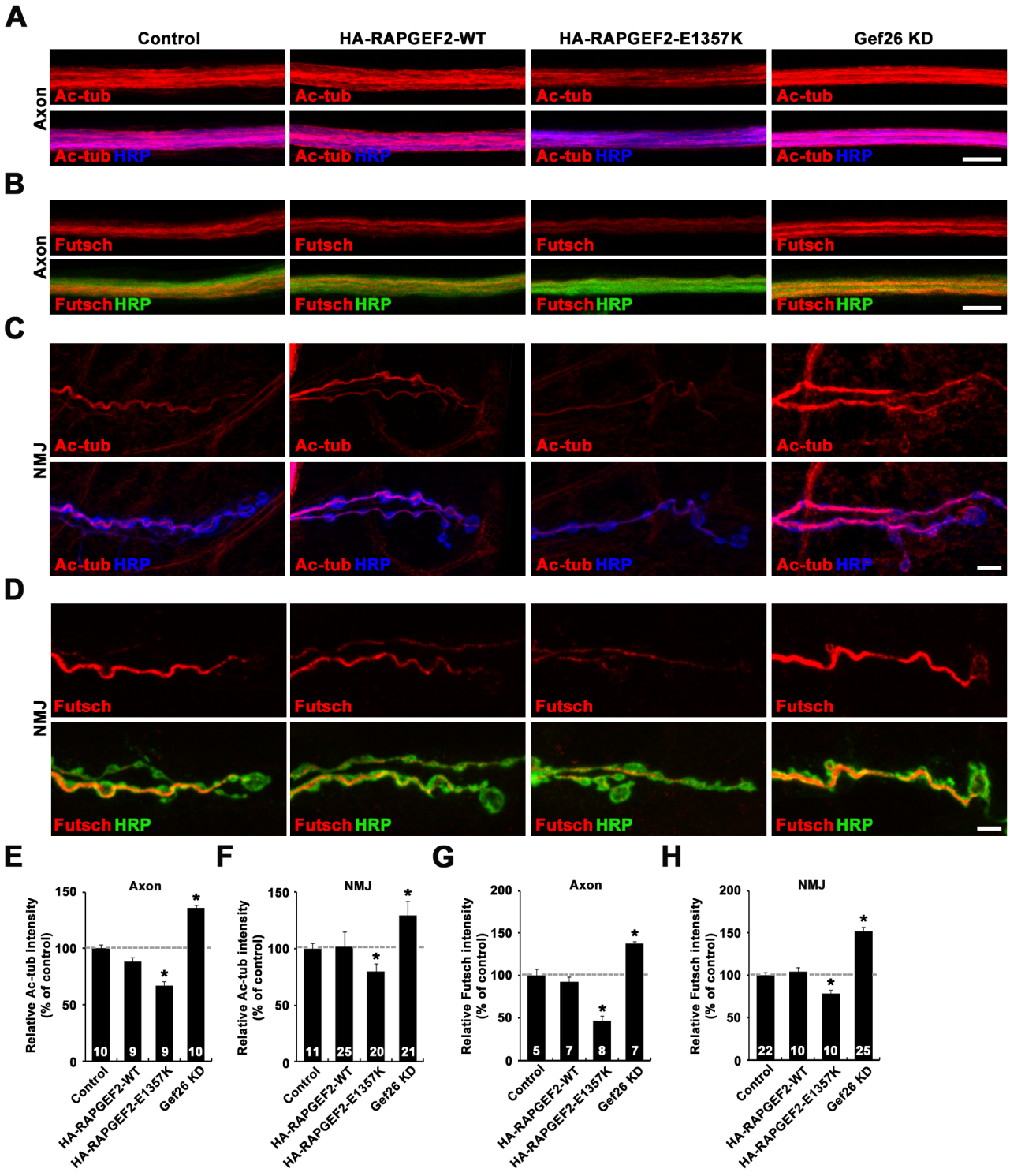

Fig. 4. Overexpression of the human RAPGEF2-E1357K variant in *Drosophila* motor neurons impairs microtubule stability in axons and at NMJ terminals. (A~D) Confocal images of motor axons (A and B) and NMJ terminals (C and D) of abdominal segment 5 in third instar larvae doubly labeled with anti-acetylated α-tubulin (Ac-tub) or anti-Futsch and anti-HRP antibodies. Genotypes include *D42-GAL4*/+ (control), *D42-GAL4*/*UAS-HA-RAPGEF2-WT* (HA-RAPGEF2-WT), *UAS-HA-RAPGEF2-E1357K*/+; *D42-GAL4*/+ (HA-RAPGEF2-E1357K), and *D42-GAL4*/*UAS-gef26*^{RNAi} (Gef26 KD). Scale bars, 5 μm. (E and F) Quantification of the ratios of mean Ac-tub to HRP fluorescence intensities in axons (E) and at NMJ terminals (F). (G and H) Quantification of the ratios of mean Futsch to HRP fluorescence intensities in axons (G) and at NMJ terminals (H). Data are presented as mean±SEM. All comparisons are made with the *D42-GAL4*/+ control (*p<0.001).

https://doi.org/10.5607/en.2018.27.6.550

by HA-RAPGEF2-WT overexpression (Fig. 4A~H). However, levels of both markers were significantly reduced in motor axons and NMJ synapses in larvae overexpressing HA-RAPGEF2-E1357K (Fig. 4A~H). These results suggest that expression of the RAPGEF2-E1357K mutation deleteriously impacts microtubule stability through a toxic gain-of-function mechanism rather than a simple dose-dependent mechanism. Next, we compared the distribution of Mito-GFP-labeled mitochondria in the soma and at the terminals of motor neurons in control larvae and larvae expressing HA-RAPGEF2-WT or HA-RAPGEF2-E1357K. The levels and distribution of Mito-GFP in the soma of motor neurons were not significantly different between the three genotypes (Fig. 5A). However, mitochondria number and area in motor axons were significantly reduced in HA-RAPGEF2-E1357K-expressing larvae compared with control or HA-RAPGEF2-WT-expressing larvae (Fig. 5B~E). We also observed a similar reduction in the area of mitochondria in NMJ synapses of HA-RAPGEF2-E1357K-expressing larvae (Fig. 5C and F). The aggregated distribution of mitochondria precluded comparison of mitochondria number in NMJ synapses.

We have recently shown that loss of the *Drosophila* RAPGEF2 homolog (Gef26) causes an increase of axonal Futsch staining [24]. To confirm this and to preclude the possibility that the E1357K mutation exerts its deleterious effect on mitochondria distribution through a loss-of-function mechanism, we depleted expression of Gef26 in motor neurons using a transgenic RNA interference (RNAi) approach. We first confirmed an increase of both acetylated α-tubulin and Futsch staining in motor axons and NMJ synapses in Gef26-knockdowned larvae (Fig. 4A~H). We found no obvious changes in the levels and distribution of mitochondria in the soma and at the terminals of motor neurons (Fig. 5A~F). These results support the notion that the RAPGEF2-E1357K mutation deleteriously impact mitochondria distribution through a toxic gain-of-function mechanism.

To test if expression of the RAPGEF2-E1357K mutant induces motor dysfunction, we performed climbing assays on adult flies at 20 days of age. Compared with transgenic controls (*D42-GAL4*/+), flies expressing *UAS-HA-RAPGEF2-WT* in motor neurons under the control of *D42-GAL4* (*D42-GAL4/UAS-HA-RAPGEF2-WT*) displayed normal climbing ability (*D42-GAL4*/+: 20.56±0.22 cm; *D42-GAL4*/*UAS-HA-RAPGEF2-WT*: 20.04±0.29 cm; $p>0.05$; Fig. 5G and H). However, age-matched flies expressing the RAPGEF2-E1357K variant made relatively short climbs (16.98±0.47 cm; $p<0.01$ from *D42-GAL4*/+; Fig. 5G and H), demonstrating the toxic effect of the human RAPGEF2-E1357K variant in *Drosophila* motor neurons.

Defective mitochondrial ultrastructure and function in patient fibroblasts

To investigate the effects of the RAPGEF2-E1357K variant on mitochondrial structures, we performed transmission electron microscopy (EM) for control and patient fibroblasts. Control mitochondria showed a typical crista structure with electron-dense deposits in the matrix (Fig. 6A). In contrast, patient fibroblasts displayed swollen and vacuolated mitochondria without lamella cristae and electron-dense deposits (Fig. 6A).

To investigate whether the ultrastructural mitochondrial abnormalities in patient fibroblasts are paralleled with mitochondrial dysfunction, we assessed mitochondrial membrane potential using JC-1, a cationic lipophilic dye. The JC-1 dye accumulates as red-fluorescent J-aggregates within mitochondria at high membrane potentials (energized mitochondria), while it accumulates as green fluorescent monomers within mitochondria at low membrane potentials (deenergized mitochondria) [36]. In live control fibroblasts loaded with JC-1, we observed strong red fluorescent signals but not green fluorescent signals (Fig. 6B), suggesting the majority of mitochondria are functional. In contrast, both red and green fluorescent signals were prominent in JC-1-loaded patient fibroblasts (Fig. 6B). These results suggest that mitochondria activity is lower in patient fibroblasts than in control fibroblasts.

Abnormal translocation of BAX to mitochondria in patient fibroblasts is rescued by pharmacological inhibition of HDAC6

Mitochondrial dysfunction is intimately linked to apoptotic cell death, which involves the mitochondrial recruitment of the proapoptotic regulator BAX from the cytosol [37]. We therefore examined whether mitochondrial dysfunction in patient-derived skin fibroblasts is paralleled with abnormal accumulation of BAX on the mitochondria. To this end, we transfected control and patient fibroblasts with a GFP-BAX construct and stained them with anti-GFP and anti-mitochondria. In control fibroblasts, BAX showed a diffuse cytoplasmic distribution with a minimal overlap with mitochondria (Fig. 7A). Notably, we observed a prominent overlap between BAX signals and mitochondria in patient fibroblasts (Fig. 7A). As an additional approach, we separated cytosolic and mitochondrial fractions from lysates of control and patient fibroblasts and performed Western blot analysis of these fractions using anti-BAX. This experiment demonstrated that BAX was more recruited to the mitochondria in patient fibroblasts than in control fibroblasts (Fig. 7B and C). In a control experiment, we confirmed that total BAX levels were comparable between control and patient derived fibroblasts (data not shown). Finally, we found that the abnormal accumulation of BAX at the mitochondria was

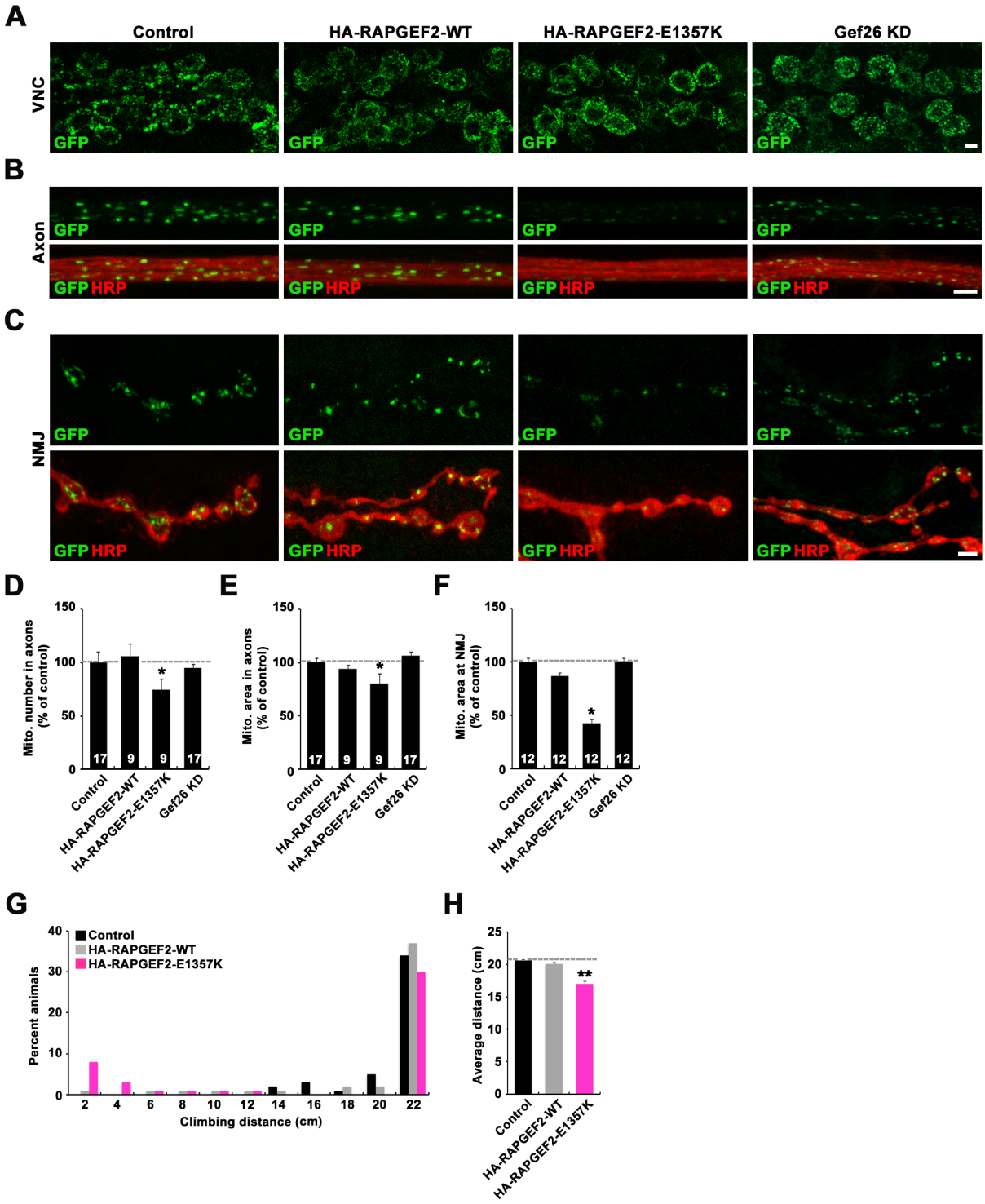

Fig. 5. Overexpression of the human RAPGEF2-E1357K variant in *Drosophila* motor neurons disrupts the distribution of mitochondria to axons and NMJ terminals. (A~C) Confocal images of ventral nerve cord (VNC, A), axon (B), and NMJ 6/7 (C) in third instar larvae stained with anti-GFP alone (A) or together with anti-HRP (B and C). Axons and NMJs in abdominal segment 5 were analyzed. Genotypes include *D42-GAL4,UAS-mito-GFP*/+ (control), *D42-GAL4,UAS-mito-GFP/UAS-HA-RAPGEF2-WT* (HA-RAPGEF2-WT), *UAS-HA-RAPGEF2-E1357K*/+; *D42-GAL4,UAS-mito-GFP*/+ (HA-RAPGEF2-E1357K), and *D42-GAL4,UAS-mito-GFP*/*UAS-gef26*^{RNAi} (Gef26 KD). Scale bars, 5 μm. (D~F) Quantification of the number (D) and area (E and F) of Mito-GFP-positive puncta in axons (D and E) and at NMJ terminals (F). Values were normalized to the respective area of axon or NMJ terminals. (G) Distribution of the distance climbed by 20-day-old *D42-GAL4*/+ (control), *D42-GAL4*/*UAS-HA-RAPGEF2-WT* (HA-RAPGEF2-WT), and *UAS-HA-RAPGEF2-E1357K*/+; *D42-GAL4*/+ (HA-RAPGEF2-E1357K) flies over 30 s. (H) Quantification of average climbing distance. Data are presented as mean±SEM. All comparisons are made with the *D42-GAL4,UAS-mito-GFP*/+ control (*p<0.001; **p<0.01).

https://doi.org/10.5607/en.2018.27.6.550

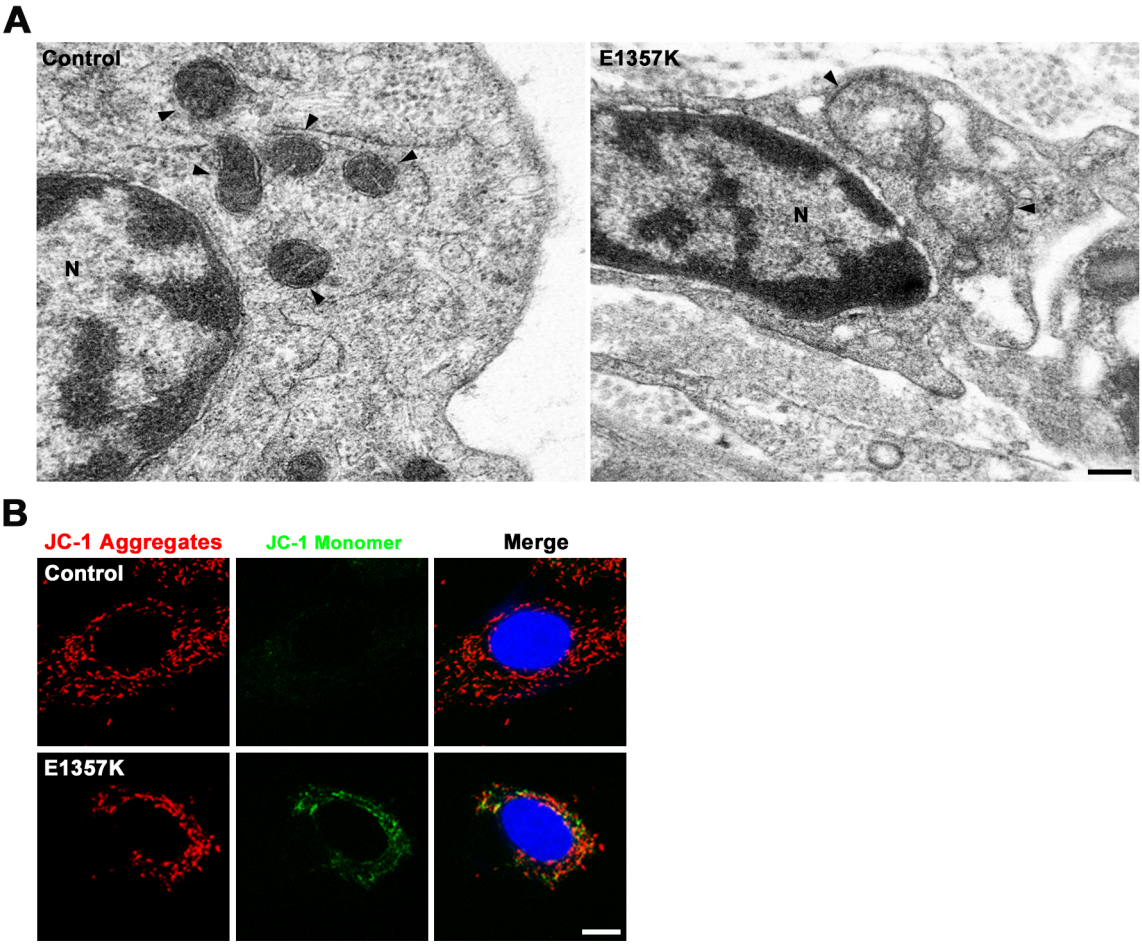

Fig. 6. Abnormalities in mitochondrial ultrastructure and function in ALS patient-derived fibroblasts. (A) Transmission electron micrographs of cross-sectioned control and patient fibroblasts. N indicates the nucleus, and arrowheads indicate mitochondria. Note that patient fibroblasts show enlarged mitochondria without cristae structures. Scale bar, 0.2 μm. (B) Fluorescent images of JC-1-loaded control and patient (E1357K) fibroblasts. Note abnormal accumulation of green-fluorescent JC-1 monomers in the mitochondria of patient but not control cells. Scale bar, 15 μm.

rescued by inhibiting HDAC6 with 1 μM tubastatin A (Fig. 7A~C). The same dose of tubastatin A had no effect on the BAX distribution in control-derived fibroblasts (Fig. 7A~C).

DISCUSSION

In this study, we report the identification of a *de novo* variant of the *RAPGEF2* gene (c.4069G>A, p.E1357K) in a patient with sALS through a trio-based WES approach. To assess the pathogenic potential of the RAPGEF2-E1357K variant, we have used skin fibroblasts derived from the patient and a *Drosophila* model carrying a RAPGEF2-E1357K transgene. In this way, we have investigated the effects of the *RAPGEF2* variant on the microtubule cytoskeleton and the mitochondria, two cellular components that are frequently affected in ALS [22, 38]. The patient fibroblasts exhibit reduction of stable microtubules as well as abnormal distribution and fragmentation of the mitochondrial network. Overexpression of the RAPGEF2-E1357K variant in *Drosophila* motor neurons impairs microtubule stability and mitochondrial distribution along axons and at NMJ presynaptic terminals. Aside from mitochondrial network abnormalities, disruption of mitochondrial structure including swelling, vacuolization, and loss of cristae have been also observed in various *in vitro* and *in vivo* models of ALS [38]. Our EM analysis reveals that patient fibroblasts carrying the RAPGEF-E1357K mutation also contain swollen and vacuolated mitochondria without cristae. Finally, patient fibroblasts show accumulation of nonfunctional mitochondria and induction of BAX recruitment to mitochondria, which is a key cellular event of mitochondria-dependent apoptosis [37]. Taken together, our results indicate that the *de novo* RAPGEF2-E1357K variant identified in our patient exerts deleterious effects on cells, which may be related to the pathogenesis of ALS.

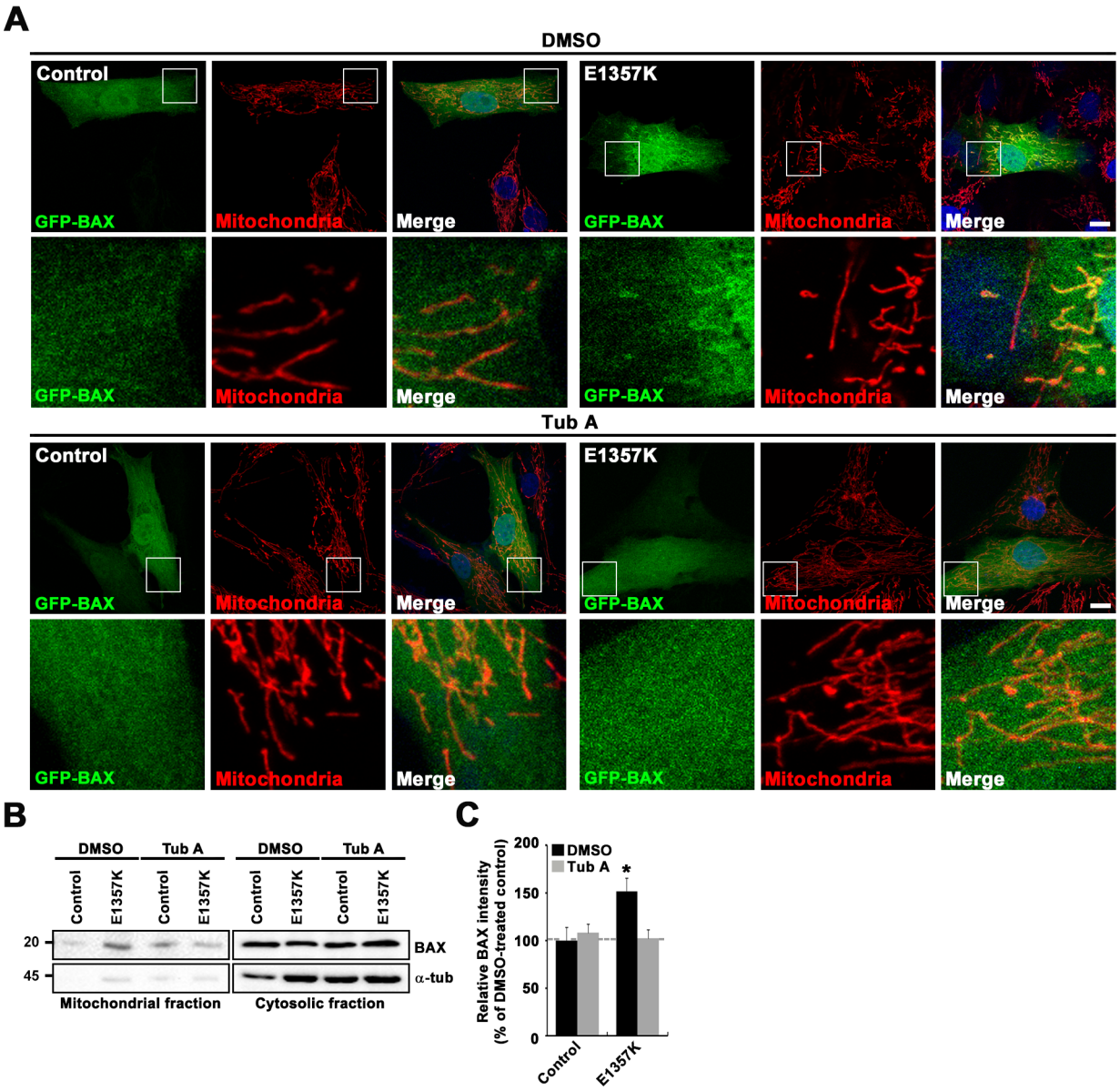

Fig. 7. Pharmacological inhibition of HDAC6 restores abnormal accumulation of BAX in the mitochondria in ALS patient-derived fibroblasts. (A) Confocal images of control and patient (E1357K) fibroblasts expressing GFP-BAX stained with anti-mitochondria antibody and DAPI. Cells were treated with DMSO or 1 μM tubastatin A (Tub A) prior to immunostaining. Scale bar, 5 μm. (B) Western blot analysis of mitochondrial and cytosolic fractions from DMSO- or Tub A-treated control and patient fibroblasts using anti-BAX and anti-α-tubulin antibodies. (C) Quantitative analysis of densitometric measurements (n=3). The band intensities of BAX in each fraction were normalized to the sum of mitochondrial and cytosolic BAX intensities. Data are presented as mean±SEM. Comparisons are made with the DMSO-treated control (*p<0.001).

Microtubules are dynamic polymers that undergo polymerization and depolymerization of α- and β-tubulin heterodimer. While developing neurons keep microtubules in a highly dynamic state during process outgrowth, mature neurons progressively increase microtubule stability to maintain many aspects of cellular functions [39, 40]. This change in microtubule stability is associated with chemical modifications of microtubules including acetylation [39]. Microtubule acetylation and deacetylation mainly occur at the conserved lysine 40 residue of α-tubulin by α-tubulin acetyltransferase 1 (αTAT1) and histone deacetylase 6 (HDAC6), respectively [34, 41]. Interestingly, several studies have demonstrated HDAC6-mediated modulation of ALS pathogenesis. For example, removal of the *HDAC6* gene is shown to delay disease progression in the SOD1-G93A mouse model of ALS [42]. More recently, it has been reported that pharmacological inhibition of HDAC6 rescues axonal transport defects in FUS-ALS patient-derived mo-

https://doi.org/10.5607/en.2018.27.6.550

tor neurons [43]. Here we show that pharmacological inhibition of HDAC6 is able to rescue both morphological mitochondria defects and abnormal accumulation of BAX in the mitochondria in patient fibroblasts carrying the RAPGEF2-E1357K variant. Thus, this study supports the notion that dysregulation of microtubule stability could act as a primary driver for ALS pathophysiology.

Consistent with our previous findings [24], knockdown of a *Drosophila* RAPGEF2 homolog (Gef26) increases the levels of acetylated α-tubulin and Futsch/MAP1B in motor axons. These phenotypes are the opposites of those induced by overexpression of the human RAFGEF2-E1357K variant in *Drosophila* motor neurons, precluding the possibility that the RAPGEF2 mutant exerts a deleterious effect on microtubule stability through a dominant negative mechanism. Moreover, overexpression of wild-type human RAPGEF2 in *Drosophila* motor neurons has no effect on axonal microtubule stability, further suggesting that the RAPGEF2-E1357K mutant impairs microtubule stability through a toxic gain-of-function mechanism rather than a simple dose-dependent mechanism.

In conclusion, we identified a *de novo RAPGEF2* variant in a sALS patient, which causes dysregulation of microtubule stability as well as of the distribution, structure, and function of mitochondria. Since these defects are becoming increasingly recognized as core components of ALS pathogenesis [22, 38], the current study warrants re-sequencing this gene in larger ALS cohorts to validate the pathogenicity of mutations in *RAPGEF2*.

ACKNOWLEDGEMENTS

This work was supported by grants from the National Research Foundation of Korea (2017M3C7A1025368 to S.L.; 2017M3C7A1025366 to C.S.K; 2017R1A6A3A04012311 to S.M.L) and by the BK21+ program of the National Research Foundation of Korea (to K.H.).

REFERENCES

1. Robberecht W, Philips T (2013) The changing scene of amyotrophic lateral sclerosis. Nat Rev Neurosci 14:248-264.
2. Taylor JP, Brown RH Jr, Cleveland DW (2016) Decoding ALS: from genes to mechanism. Nature 539:197-206.
3. Renton AE, Chiò A, Traynor BJ (2014) State of play in amyotrophic lateral sclerosis genetics. Nat Neurosci 17:17-23.
4. Müller K, Brenner D, Weydt P, Meyer T, Grehl T, Petri S, Grosskreutz J, Schuster J, Volk AE, Borck G, Kubisch C, Klopstock T, Zeller D, Jablonka S, Sendtner M, Klebe S, Knehr A, Günther K, Weis J, Claeys KG, Schrank B, Sperfeld AD, Hübers A, Otto M, Dorst J, Meitinger T, Strom TM, Andersen PM, Ludolph AC, Weishaupt JH; German ALS network MND-NET (2018) Comprehensive analysis of the mutation spectrum in 301 German ALS families. J Neurol Neurosurg Psychiatry 89:817-827.
5. Leblond CS, Kaneb HM, Dion PA, Rouleau GA (2014) Dissection of genetic factors associated with amyotrophic lateral sclerosis. Exp Neurol 262 Pt B:91-101.
6. De Vos KJ, Hafezparast M (2017) Neurobiology of axonal transport defects in motor neuron diseases: opportunities for translational research? Neurobiol Dis 105:283-299.
7. Sasaki S, Iwata M (2007) Mitochondrial alterations in the spinal cord of patients with sporadic amyotrophic lateral sclerosis. J Neuropathol Exp Neurol 66:10-16.
8. De Vos KJ, Chapman AL, Tennant ME, Manser C, Tudor EL, Lau KF, Brownlees J, Ackerley S, Shaw PJ, McLoughlin DM, Shaw CE, Leigh PN, Miller CC, Grierson AJ (2007) Familial amyotrophic lateral sclerosis-linked SOD1 mutants perturb fast axonal transport to reduce axonal mitochondria content. Hum Mol Genet 16:2720-2728.
9. Sotelo-Silveira JR, Lepanto P, Elizondo V, Horjales S, Palacios F, Martinez-Palma L, Marin M, Beckman JS, Barbeito L (2009) Axonal mitochondrial clusters containing mutant SOD1 in transgenic models of ALS. Antioxid Redox Signal 11:1535-1545.
10. Magrané J, Sahawneh MA, Przedborski S, Estévez AG, Manfredi G (2012) Mitochondrial dynamics and bioenergetic dysfunction is associated with synaptic alterations in mutant SOD1 motor neurons. J Neurosci 32:229-242.
11. Wang W, Li L, Lin WL, Dickson DW, Petrucelli L, Zhang T, Wang X (2013) The ALS disease-associated mutant TDP-43 impairs mitochondrial dynamics and function in motor neurons. Hum Mol Genet 22:4706-4719.
12. Daoud H, Zhou S, Noreau A, Sabbagh M, Belzil V, Dionne-Laporte A, Tranchant C, Dion P, Rouleau GA (2012) Exome sequencing reveals SPG11 mutations causing juvenile ALS. Neurobiol Aging 33:839.e5-839.e9.
13. Klein CJ, Wu Y, Duan X, Middha S, Dawson BD, Kocher JP, Dyck PJ (2013) Novel SOD1 mutation discovered in atypical ALS by whole exome sequencing. J Neurol Neurosurg Psychiatry 84:943-944.
14. Williams KL, Warraich ST, Yang S, Solski JA, Fernando R, Rouleau GA, Nicholson GA, Blair IP (2012) UBQLN2/ubiquilin 2 mutation and pathology in familial amyotrophic lateral sclerosis. Neurobiol Aging 33:2527.e3-2527.e10.
15. Johnson JO, Mandrioli J, Benatar M, Abramzon Y, Van Deerlin VM, Trojanowski JQ, Gibbs JR, Brunetti M, Gronka S,

Wuu J, Ding J, McCluskey L, Martinez-Lage M, Falcone D, Hernandez DG, Arepalli S, Chong S, Schymick JC, Rothstein J, Landi F, Wang YD, Calvo A, Mora G, Sabatelli M, Monsurrò MR, Battistini S, Salvi F, Spataro R, Sola P, Borghero G, Galassi G, Scholz SW, Taylor JP, Restagno G, Chiò A, Traynor BJ; ITALSGEN Consortium (2010) Exome sequencing reveals VCP mutations as a cause of familial ALS. Neuron 68:857-864.

16. Kim HJ, Kim NC, Wang YD, Scarborough EA, Moore J, Diaz Z, MacLea KS, Freibaum B, Li S, Molliex A, Kanagaraj AP, Carter R, Boylan KB, Wojtas AM, Rademakers R, Pinkus JL, Greenberg SA, Trojanowski JQ, Traynor BJ, Smith BN, Topp S, Gkazi AS, Miller J, Shaw CE, Kottlors M, Kirschner J, Pestronk A, Li YR, Ford AF, Gitler AD, Benatar M, King OD, Kimonis VE, Ross ED, Weihl CC, Shorter J, Taylor JP (2013) Mutations in prion-like domains in hnRNPA2B1 and hnRNPA1 cause multisystem proteinopathy and ALS. Nature 495:467-473.
17. Wu CH, Fallini C, Ticozzi N, Keagle PJ, Sapp PC, Piotrowska K, Lowe P, Koppers M, McKenna-Yasek D, Baron DM, Kost JE, Gonzalez-Perez P, Fox AD, Adams J, Taroni F, Tiloca C, Leclerc AL, Chafe SC, Mangroo D, Moore MJ, Zitzewitz JA, Xu ZS, van den Berg LH, Glass JD, Siciliano G, Cirulli ET, Goldstein DB, Salachas F, Meininger V, Rossoll W, Ratti A, Gellera C, Bosco DA, Bassell GJ, Silani V, Drory VE, Brown RH Jr, Landers JE (2012) Mutations in the profilin 1 gene cause familial amyotrophic lateral sclerosis. Nature 488:499-503.
18. Cirulli ET, Lasseigne BN, Petrovski S, Sapp PC, Dion PA, Leblond CS, Couthouis J, Lu YF, Wang Q, Krueger BJ, Ren Z, Keebler J, Han Y, Levy SE, Boone BE, Wimbish JR, Waite LL, Jones AL, Carulli JP, Day-Williams AG, Staropoli JF, Xin WW, Chesi A, Raphael AR, McKenna-Yasek D, Cady J, Vianney de Jong JM, Kenna KP, Smith BN, Topp S, Miller J, Gkazi A, Al-Chalabi A, van den Berg LH, Veldink J, Silani V, Ticozzi N, Shaw CE, Baloh RH, Appel S, Simpson E, Lagier-Tourenne C, Pulst SM, Gibson S, Trojanowski JQ, Elman L, McCluskey L, Grossman M, Shneider NA, Chung WK, Ravits JM, Glass JD, Sims KB, Van Deerlin VM, Maniatis T, Hayes SD, Ordureau A, Swarup S, Landers J, Baas F, Allen AS, Bedlack RS, Harper JW, Gitler AD, Rouleau GA, Brown R, Harms MB, Cooper GM, Harris T, Myers RM, Goldstein DB; FALS Sequencing Consortium (2015) Exome sequencing in amyotrophic lateral sclerosis identifies risk genes and pathways. Science 347:1436-1441.
19. Kenna KP, van Doormaal PT, Dekker AM, Ticozzi N, Kenna BJ, Diekstra FP, van Rheenen W, van Eijk KR, Jones AR, Keagle P, Shatunov A, Sproviero W, Smith BN, van Es MA, Topp SD, Kenna A, Miller JW, Fallini C, Tiloca C, McLaughlin RL, Vance C, Troakes C, Colombrita C, Mora G, Calvo A, Verde F, Al-Sarraj S, King A, Calini D, de Belleroche J, Baas F, van der Kooi AJ, de Visser M, Ten Asbroek AL, Sapp PC, McKenna-Yasek D, Polak M, Asress S, Muñoz-Blanco JL, Strom TM, Meitinger T, Morrison KE, Lauria G, Williams KL, Leigh PN, Nicholson GA, Blair IP, Leblond CS, Dion PA, Rouleau GA, Pall H, Shaw PJ, Turner MR, Talbot K, Taroni F, Boylan KB, Van Blitterswijk M, Rademakers R, Esteban-Pérez J, García-Redondo A, Van Damme P, Robberecht W, Chio A, Gellera C, Drepper C, Sendtner M, Ratti A, Glass JD, Mora JS, Basak NA, Hardiman O, Ludolph AC, Andersen PM, Weishaupt JH, Brown RH Jr, Al-Chalabi A, Silani V, Shaw CE, van den Berg LH, Veldink JH, Landers JE; SLAGEN Consortium (2016) NEK1 variants confer susceptibility to amyotrophic lateral sclerosis. Nat Genet 48:1037-1042.
20. Chesi A, Staahl BT, Jovičić A, Couthouis J, Fasolino M, Raphael AR, Yamazaki T, Elias L, Polak M, Kelly C, Williams KL, Fifita JA, Maragakis NJ, Nicholson GA, King OD, Reed R, Crabtree GR, Blair IP, Glass JD, Gitler AD (2013) Exome sequencing to identify de novo mutations in sporadic ALS trios. Nat Neurosci 16:851-855.
21. Steinberg KM, Yu B, Koboldt DC, Mardis ER, Pamphlett R (2015) Exome sequencing of case-unaffected-parents trios reveals recessive and de novo genetic variants in sporadic ALS. Sci Rep 5:9124.
22. Clark JA, Yeaman EJ, Blizzard CA, Chuckowree JA, Dickson TC (2016) A case for microtubule vulnerability in amyotrophic lateral sclerosis: altered dynamics during disease. Front Cell Neurosci 10:204.
23. Lim SM, Choi WJ, Oh KW, Xue Y, Choi JY, Kim SH, Nahm M, Kim YE, Lee J, Noh MY, Lee S, Hwang S, Ki CS, Fu XD, Kim SH (2016) Directly converted patient-specific induced neurons mirror the neuropathology of FUS with disrupted nuclear localization in amyotrophic lateral sclerosis. Mol Neurodegener 11:8.
24. Heo K, Nahm M, Lee MJ, Kim YE, Ki CS, Kim SH, Lee S (2017) The Rap activator Gef26 regulates synaptic growth and neuronal survival via inhibition of BMP signaling. Mol Brain 10:62.
25. Babic M, Russo GJ, Wellington AJ, Sangston RM, Gonzalez M, Zinsmaier KE (2015) Miro's N-terminal GTPase domain is required for transport of mitochondria into axons and dendrites. J Neurosci 35:5754-5771.
26. Rana A, Seinen E, Siudeja K, Muntendam R, Srinivasan B, van der Want JJ, Hayflick S, Reijngoud DJ, Kayser O, Sibon OC

(2010) Pantethine rescues a Drosophila model for pantothenate kinase-associated neurodegeneration. Proc Natl Acad Sci U S A 107:6988-6993.
27. Brooks BR, Miller RG, Swash M, Munsat TL; World Federation of Neurology Research Group on Motor Neuron Diseases (2000) El Escorial revisited: revised criteria for the diagnosis of amyotrophic lateral sclerosis. Amyotroph Lateral Scler Other Motor Neuron Disord 1:293-299.
28. Mackenzie IR, Nicholson AM, Sarkar M, Messing J, Purice MD, Pottier C, Annu K, Baker M, Perkerson RB, Kurti A, Matchett BJ, Mittag T, Temirov J, Hsiung GR, Krieger C, Murray ME, Kato M, Fryer JD, Petrucelli L, Zinman L, Weintraub S, Mesulam M, Keith J, Zivkovic SA, Hirsch-Reinshagen V, Roos RP, Züchner S, Graff-Radford NR, Petersen RC, Caselli RJ, Wszolek ZK, Finger E, Lippa C, Lacomis D, Stewart H, Dickson DW, Kim HJ, Rogaeva E, Bigio E, Boylan KB, Taylor JP, Rademakers R (2017) TIA1 mutations in amyotrophic lateral sclerosis and frontotemporal dementia promote phase separation and alter stress granule dynamics. Neuron 95:808-816.e9.
29. Molliex A, Temirov J, Lee J, Coughlin M, Kanagaraj AP, Kim HJ, Mittag T, Taylor JP (2015) Phase separation by low complexity domains promotes stress granule assembly and drives pathological fibrillization. Cell 163:123-133.
30. Patel A, Lee HO, Jawerth L, Maharana S, Jahnel M, Hein MY, Stoynov S, Mahamid J, Saha S, Franzmann TM, Pozniakovski A, Poser I, Maghelli N, Royer LA, Weigert M, Myers EW, Grill S, Drechsel D, Hyman AA, Alberti S (2015) A liquid-to-solid phase transition of the ALS protein FUS accelerated by disease mutation. Cell 162:1066-1077.
31. Webster DR, Borisy GG (1989) Microtubules are acetylated in domains that turn over slowly. J Cell Sci 92:57-65.
32. Vadlamudi RK, Barnes CJ, Rayala S, Li F, Balasenthil S, Marcus S, Goodson HV, Sahin AA, Kumar R (2005) p21-activated kinase 1 regulates microtubule dynamics by phosphorylating tubulin cofactor B. Mol Cell Biol 25:3726-3736.
33. d'Ydewalle C, Krishnan J, Chiheb DM, Van Damme P, Irobi J, Kozikowski AP, Vanden Berghe P, Timmerman V, Robberecht W, Van Den Bosch L (2011) HDAC6 inhibitors reverse axonal loss in a mouse model of mutant HSPB1-induced Charcot-Marie-Tooth disease. Nat Med 17:968-974.
34. Hubbert C, Guardiola A, Shao R, Kawaguchi Y, Ito A, Nixon A, Yoshida M, Wang XF, Yao TP (2002) HDAC6 is a microtubule-associated deacetylase. Nature 417:455-458.
35. Roos J, Hummel T, Ng N, Klämbt C, Davis GW (2000) Drosophila Futsch regulates synaptic microtubule organization and is necessary for synaptic growth. Neuron 26:371-382.
36. Smiley ST, Reers M, Mottola-Hartshorn C, Lin M, Chen A, Smith TW, Steele GD Jr, Chen LB (1991) Intracellular heterogeneity in mitochondrial membrane potentials revealed by a J-aggregate-forming lipophilic cation JC-1. Proc Natl Acad Sci U S A 88:3671-3675.
37. Lindsay J, Esposti MD, Gilmore AP (2011) Bcl-2 proteins and mitochondria--specificity in membrane targeting for death. Biochim Biophys Acta 1813:532-539.
38. Smith EF, Shaw PJ, De Vos KJ (2017) The role of mitochondria in amyotrophic lateral sclerosis. Neurosci Lett (in press).
39. Ferreira A, Cáceres A (1989) The expression of acetylated microtubules during axonal and dendritic growth in cerebellar macroneurons which develop in vitro. Brain Res Dev Brain Res 49:205-213.
40. Lim SS, Sammak PJ, Borisy GG (1989) Progressive and spatially differentiated stability of microtubules in developing neuronal cells. J Cell Biol 109:253-263.
41. Akella JS, Wloga D, Kim J, Starostina NG, Lyons-Abbott S, Morrissette NS, Dougan ST, Kipreos ET, Gaertig J (2010) MEC-17 is an alpha-tubulin acetyltransferase. Nature 467:218-222.
42. Taes I, Timmers M, Hersmus N, Bento-Abreu A, Van Den Bosch L, Van Damme P, Auwerx J, Robberecht W (2013) Hdac6 deletion delays disease progression in the SOD1G93A mouse model of ALS. Hum Mol Genet 22:1783-1790.
43. Guo W, Naujock M, Fumagalli L, Vandoorne T, Baatsen P, Boon R, Ordovás L, Patel A, Welters M, Vanwelden T, Geens N, Tricot T, Benoy V, Steyaert J, Lefebvre-Omar C, Boesmans W, Jarpe M, Sterneckert J, Wegner F, Petri S, Bohl D, Vanden Berghe P, Robberecht W, Van Damme P, Verfaillie C, Van Den Bosch L (2017) HDAC6 inhibition reverses axonal transport defects in motor neurons derived from FUS-ALS patients. Nat Commun 8:861.